Monthly Notices
of the
ROYAL ASTRONOMICAL SOCIETY

MNRAS **449,** 3137–3148 (2015) doi:10.1093/mnras/stv494

Galaxy formation with radiative and chemical feedback

L. Graziani,[1⋆] S. Salvadori,[2] R. Schneider,[1] D. Kawata,[3] M. de Bennassuti[1] and A. Maselli[4]

[1]*INAF Osservatorio Astronomico di Roma, Via Frascati 33, I-00040, Monte Porzio Catone (RM), Italy*
[2]*Kapteyn Astronomical Institute, Landleven 12, NL-9747 AD Groningen, the Netherlands*
[3]*Mullard Space Science Laboratory, University College London, Holmbury St Mary, Dorking, Surrey, RH5 6NT, UK*
[4]*EVENT Lab for Neuroscience and Technology, Universitat de Barcelona, Passeig de la Vall d'Hebron 171, E-08035 Barcelona, Spain*

Accepted 2015 March 4. Received 2015 February 24; in original form 2014 November 30

ABSTRACT

Here we introduce GAMESH, a novel pipeline that implements self-consistent radiative and chemical feedback in a computational model of galaxy formation. By combining the cosmological chemical-evolution model GAMETE with the radiative transfer code CRASH, GAMESH can post-process realistic outputs of a *N*-body simulation describing the red-shift evolution of the forming galaxy. After introducing the GAMESH implementation and its features, we apply the code to a low-resolution *N*-body simulation of the formation of the Milky Way and we investigate the combined effects of self-consistent radiative and chemical feedback. Many physical properties, which can be directly compared with observations in the Galaxy and its surrounding satellites, are predicted by the code along with the merger-tree assembly. The resulting red-shift evolution for the Local Group of star-formation rates, reionization and metal enrichment along with the predicted metallicity distribution function of halo stars are critically compared with observations. We discuss the merits and limitations of the first release of GAMESH, which also opens new directions to a full implementation of feedback processes in galaxy-formation models by combining semi-analytic and numerical methods.

Key words: stars: formation – stars: Population II – galaxies: evolution – galaxies: formation – galaxies: stellar content – cosmology: theory.

1 INTRODUCTION

Since the pioneering work of Couchman & Rees (1986), the radiative feedback induced by cosmic reionization has been recognized to have a strong impact on the formation and evolution of galaxies (Gnedin 2000; Benson et al. 2002a,b; Somerville 2002; Hoeft et al. 2006; Okamoto, Gao & Theuns 2008; Salvadori & Ferrara 2009; Lunnan et al. 2012; Sawala et al. 2014), imprinting specific signatures in the observed properties of the local Universe (Brown et al. 2012).

Semi-analytic models of galaxy formation (see e.g. Benson et al. 2002a,b or Somerville 2002) and numerical simulations, both unidimensional (Thoul & Weinberg 1996; Kitayama et al. 2000; Dijkstra et al. 2004; Sobacchi & Mesinger 2013) and three-dimensional (see Gnedin 2000; Hoeft et al. 2006; Okamoto et al. 2008 and references therein) have been performed to determine the efficiency of the radiative feedback and the way it affects galactic star formation (SF) by either an extended (*gradual*) or instant (*sharp*) process in red shift; however a physically motivated prescription is still missing (Noh & McQuinn 2014). Models with a sharp SF suppression after reionization generally fail to reproduce the present, observed luminosity function and predict an unacceptable gap between the faint and the bright populations, also showing that a red-shift dependence in modelling feedback effects is necessary. The value of the critical mass below which galaxies should be strongly affected by photo-ionization at fixed red shift is also subject to an intense debate: recent numerical studies (Hoeft et al. 2006; Okamoto et al. 2008) find about one order of magnitude lower masses compared to the original calculations (Gnedin 2000), but all the conclusions critically depend on the reliability of the ionizing background (ultraviolet background or UVB) adopted by the semi-analytic model.

The effects of a UVB maintaining the Universe in a reionized state can be also considerable on the structure and properties of the Local Group. The tendency of numerical simulations to overpredict the substructures on small scales compared to the observed population, the so-called missing satellite problem (Moore et al. 1999; Klypin et al. 1999; Boylan-Kolchin, Bullock & Kaplinghat 2012), is often interpreted as an inability to reproduce the inefficient or suppressed SF acting in the group of local dwarf galaxies, causing small haloes to remain dark, and then invisible to observations (Alvarez et al. 2009; Busha et al. 2010; Ocvirk et al. 2014). Feedback processes have been invoked to justify this failure of the cold

⋆E-mail: luca.graziani@oa-roma.inaf.it

dark matter (ΛCDM) model, both mechanical (Kravtsov, Gnedin & Klypin 2004; D'Onghia et al. 2009, 2010) and radiative (Efstathiou 1992; Gnedin 2000; Benson et al. 2002a; Somerville 2002; Madau et al. 2008; Noh & McQuinn 2014; Milosavljević & Bromm 2014).

A correct determination of the epoch of hydrogen reionization on the scale of galaxy formation, self-consistently with the SF suppression operated by radiative feedback, could shed some light also on the nature of the ultra-faint dwarf population found in the Sloan Digital Sky Survey (SDSS, Willman et al. 2005; Belokurov et al. 2006; Zucker et al. 2006a,b). The discovery of these galaxies, roughly doubling the number of known Milky Way (MW) satellites, forced an update of the old models and opened new questions on whether this population is made by pre-reionization fossils or it is just the lowest-luminosity tail of classical dwarfs. The answer will critically depend, again, on the way the gas ionization is modelled and on how radiative effects are taken into account.

By using a data-calibrated model for the formation of the MW and its dwarf satellites, which includes the presence of inefficient star-forming mini-haloes and a heuristic prescription to account for radiative feedback, Salvadori & Ferrara (2009) have been able to reproduce simultaneously the observed iron-luminosity relation and the metallicity distribution function (MDF) of nearby dwarf galaxies, including the ultra-faint population. The authors argued that ultra-faint dwarf galaxies might represent the fossil relics of a once ubiquitous population of H_2-cooling mini-haloes that formed before reionization ($z > 8.5$), similarly to what has been found by independent groups (Madau et al. 2008; Koposov et al. 2009; Bovill & Ricotti 2009; Muñoz et al. 2009; Bovill & Ricotti 2011a,b) and in agreement with a series of more recent studies (Salvadori & Ferrara 2012; Salvadori et al. 2014). In particular, they find that a gradual suppression of the SF in increasingly massive (mini-)haloes is necessary to match the observed iron-luminosity relation and the MDF of nearby dwarfs. Although this empirical relation is consistent with the minimum mass for SF settled by an advanced semi-analytic treatment of reionization (Salvadori et al. 2014), the results still rely on the assumptions made on the nature and efficiency of feedback acting on SF haloes. More detailed modelling is certainly required to understand the *local* effects of inhomogeneous radiative feedback and its impact on the luminosity function of MW satellites.

It should be noted, on the other hand, that the observed luminosity function of MW satellites is certainly not sufficient to fully constrain semi-analytic models as shown, for instance, by alternative approaches (Macciò et al. 2010; Li, De Lucia & Helmi 2010). The observed number and distribution of luminous satellites can be reproduced with accuracy also by assuming a sharp (i.e. instant) reionization and a strongly mass-dependent SF efficiency or by invoking other physical processes, such as supernovae feedback or tidal stripping.

Recent investigations (Alvarez et al. 2009; Busha et al. 2010; Lunnan et al. 2012; Li et al. 2014) have tried to advance the treatment of the radiative feedback, mainly by relaxing the assumption of a uniform reionization field (Macciò et al. 2010; Li et al. 2010). These studies generally combine the merger-tree histories of advanced *N*-body simulations (e.g. Springel et al. 2008) with semi-analytic radiative transfer (RT; see for instance Zahn et al. 2011) describing an inhomogeneous reionization process. Despite the different approaches, the population of faint satellites is always highly sensitive to the adopted reionization model.

We finally point out that the observed properties of the MW satellites in the local Universe (Salvadori & Ferrara 2009; Salvadori et al. 2014) are the result of the global interplay between radiative, mechanical and eventually chemical feedback, and a more comprehensive study is necessary to interpret the various observational signatures left during galaxy evolution: the origin and properties of the observed population of metal-poor stars in our galaxy and the low-metallicity tail of the MDF.

In this paper we introduce GAMESH, a new pipeline integrating the latest release of the cosmological RT code CRASH (Graziani, Maselli & Ciardi 2013) with the semi-analytic model of galaxy formation GAMETE, powered by an *N*-body simulation (Salvadori et al. 2010, hereafter SF10). By treating SF, metal enrichment and photo-ionization in a self-consistent way, GAMESH is an ideal tool to study the effects of photo-ionization and heating in galaxy-formation simulations and can address many of the questions discussed above. In addition, the RT model adopted by GAMESH relies on a Monte Carlo scheme and not only naturally accounts for the inhomogeneities of the ionization process, but also allows a deep investigation of other RT effects, a self-consistent calculation of the gas temperature, and a more accurate description of the stellar populations responsible for the MW environment reionization.

In the present work, the GAMESH pipeline will be applied to the Galaxy-formation simulation introduced in Scannapieco et al. (2006) and successfully post-processed by the semi-analytic code GAMETE (SF10), to derive the properties of the central galaxy and to compare them with the available observations of the MW system. Although the mass resolution of the adopted *N*-body does not provide sufficient statistics of mini-haloes to study the missing satellite problem, the robust set of results already obtained with the previous semi-analytic approach offers an excellent validation framework for the GAMESH pipeline and allows us to appreciate the many advantages of the accurate RT treatment of CRASH coupled with the semi-analytic approach of GAMETE. A future work, already in place, will focus on high-resolution simulations to address all the scientific problems discussed above with the adequate level of detail.

The paper is organized as follows. In Section 2 we describe the GAMESH pipeline by briefly introducing its components and by providing details of the feedback implementation. The MW reionization simulation is introduced in Section 3 and the results discussed in Section 4. Section 5 finally summarises the conclusions of the paper.

2 THE GAMESH PIPELINE

In this section, we describe the workflow of the GAMESH pipeline, which integrates an *N*-body simulation, the semi-analytic code GAMETE (see Section 2.1 for more details), and the RT code CRASH (see Section 2.2); more details of each pipeline module can be found in the dedicated subsections.

GAMESH models the galaxy-formation process by concatenating a series of snapshots provided by an *N*-body run at given red shifts $z_{i=0,\ldots,N}$: the pipeline uses the physical quantities calculated at z_i as initial conditions for the successive calculation at z_{i+1}. Along the red-shift evolution, the feedback between SF and RT is handled by two software modules called interactors I_0 (detailed in Section 2.3) and I_1 (see Section 2.4). I_0 transforms the galaxy star-formation rates (SFRs) predicted by GAMETE into a list of ionizing sources for CRASH, while I_1 uses the gas ionization and temperature determined by the RT to establish a SF prescription for the semi-analytic model implemented in GAMETE. Hereafter, we focus on the pipeline logic at fixed z_i (see Fig. 1); for simplicity, we also generically refer to the ionization of the gas as $x_{\rm gas}$, while a more specific notation will be adopted in Section 4 to discuss the ionization fractions of hydrogen and helium.

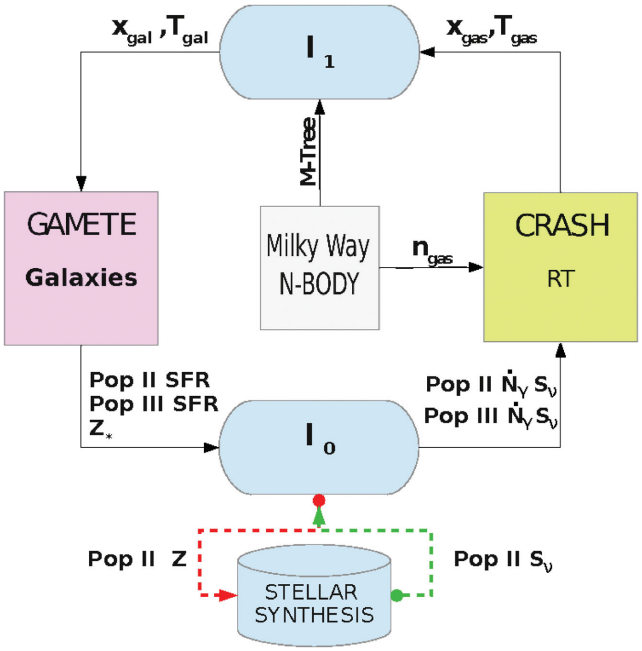

Figure 1. GAMESH pipeline logic at fixed red shift z_i. The quantities $x_{\rm gal}$, $T_{\rm gal}$, $x_{\rm gas}$ and $T_{\rm gas}$ refer to the ionization fractions and temperatures of the gas in the grid cells containing galaxies and in the simulated domain, respectively. The gas number density projected into the grid used by CRASH is indicated as $n_{\rm gas}$ and the global set of information provided by the N-body merger tree as M-Tree. The quantities used by interactor I_0 are the star-formation rates (SFRs) and the metallicity of the stars (Z_*), while the computed ionization rates and spectral shapes per galaxy and population are indicated as $\dot{N}_\gamma$ and S_ν. See text for more details.

The initial conditions of the pipeline are provided by the N-body simulation, which assigns the simulation red shift z_i to all the components, sets up the N-body merger tree into I_1 and the gas number density ($n_{\rm gas}$) in the grid used by CRASH to map the physical domain.

Once the initial conditions are set up, I_1 starts the simulation by creating a list of galaxies found in the merger tree: each galaxy is identified by a unique ID and it is associated with the values of $x_{\rm gal}$ and $T_{\rm gal}$ found in the cell of the grid containing the galaxy centre of mass (see Section 2.4 for more details). This list is then processed by GAMETE to establish which galaxies can form stars, self-consistently with the metallicity, temperature and ionization of the accreting gas.

As output of GAMETE, we obtain a sub-sample of star-forming galaxies (SFGs), their SFRs, stellar metallicity and population type. I_0 converts this sample into a list of CRASH sources by evaluating the galaxy positions on the grid, their spectrum-integrated ionization rate $\dot{N}_\gamma$ and the spectral shape S_ν. A stellar synthesis database has been implemented in I_0 (see Section 2.3) to derive $\dot{N}_\gamma$ and S_ν from the stellar metallicity and the SFR.

Once the properties of the radiating galaxies are established, the RT simulation starts propagating photons for a simulation duration corresponding to the Hubble time separating two snapshots, and it obtains the gas ionization $x_{\rm gas}$ and temperature $T_{\rm gas}$ at red shift z_i. These quantities are finally used for the subsequent red shift z_{i+1}, by repeating the same algorithm.

Before moving to a more detailed description of the GAMESH components, we want to emphasize the advantages of our approach. We first point out that CRASH allows us to follow accurately the reionization of the MW progenitors along the red-shift evolution, by taking into account the intrinsic inhomogeneities due to the gas clumps and by calculating the temperature history self-consistently. Moreover, RT effects, which generally lead to spectral hardening that may preferentially heat the gas in over-dense regions, will be accounted for by the RT simulation without pre-assuming any propagation model.

The adoption of GAMETE allows us to explore fully the interplay between reionization, radiative feedback and chemical evolution, which can have very interesting and testable consequences (Schneider et al. 2008). Using this approach, we can break the degeneracy between having gradual suppression and constant SF efficiency or sharp suppression and mass-dependent SF efficiency.

The following sections provide more details of the pipeline components.

2.1 GAMETE

GAMETE (Salvadori, Schneider & Ferrara 2007) is a data-constrained semi-analytic model for the formation of the MW and its dwarf satellites (Salvadori & Ferrara 2009). The algorithm has been designed to study the properties of the first stars and the early chemical enrichment of the Galaxy. The evolution of gas and stars inside each galactic halo of the merger-tree hierarchy (group of dark matter (DM) particles) is traced by assuming the following hypotheses:

(i) At the highest red shift of the merger tree, the gas has a primordial composition.

(ii) In each galaxy, the SFR is proportional to the mass of cold gas.

(iii) The contribution of radiative feedback is accounted for by adopting different prescriptions, depending on the problem at hand. When the code runs in stand-alone mode (i.e. not in pipeline), GAMETE assumes instant reionization (IReion, SF10), i.e. stars form only in galaxies of mass $M_h > M_4(z) = 3 \times 10^8\,{\rm M}_\odot (1+z)^{-3/2}$ ($M_h > M_{30}(z) = 2.89 \times M_4(z)$) prior to (after) reionization (assumed complete at $z = 6$). When GAMETE runs coupled with CRASH, SF is not regulated by the halo mass but by exact radiative feedback effects as predicted by the RT simulation and detailed in Section 2.4. In this case, the SF efficiency in mini-haloes (i.e. haloes with $T_{\rm vir} < 2 \times 10^4$ K) is decreased $\propto T_{\rm vir}^{-3}$ as already detailed in Salvadori & Ferrara (2012), to mimic the effects of a Lyman-Werner (LW) background.

Although recent versions of GAMETE (Salvadori et al. 2014; de Bennassuti et al. 2014) allow us to follow the Pop III to Pop II transition by accounting for detailed chemical feedback (including the dust evolution) and exploring different Pop III initial mass functions (IMFs) and stellar lifetimes, as well as the effects of the inhomogeneous distribution of metals, the first release of GAMESH implements the simplified version of the chemical network as detailed below, for better comparison with the results in SF10.

(i) According to the critical metallicity scenario (Schneider et al. 2002, 2006), low-mass stars form according to a standard Salpeter-like IMF when the gas metallicity $Z \geq Z_{\rm cr} = 10^{-4}\,{\rm Z}_\odot$; for $Z < Z_{\rm cr}$, massive Pop III stars form with a mass $m_{\rm Pop\,III} = 200\,{\rm M}_\odot$.

(ii) The enrichment of gas within the galaxies and in the diffused MW environment (MWenv) is calculated by including a simple description of supernova feedback (Salvadori, Ferrara & Schneider 2008). Metals and gas are assumed to be instantaneously and homogeneously mixed by adopting the instantaneous recycling approximation (Tinsley 1980); the implications of this choice are discussed in Salvadori et al. (2007, 2010).

The interplay between the *N*-body scheme and semi-analytic calculation, along the red-shift evolution of the simulation, is detailed below. At each time step, the mass of gas, metals and stars within each halo is equally distributed among all its DM particles, and used in the next integration step as initial conditions. The same technique is applied to metals ejected into the MWenv so that the chemical composition of newly virializing haloes depends on the enrichment level of the environment out of which they form. To recover the spatial distribution of the long-living metal-poor stars at $z = 0$, we also store their properties per DM particle.

2.2 CRASH

CRASH (Ciardi et al. 2001; Maselli, Ferrara & Ciardi 2003; Maselli & Ferrara 2005; Maselli, Ciardi & Kanekar 2009; Graziani et al. 2013) is a Monte Carlo based scheme implementing 3D ray tracing of ionizing radiation through a gas composed of H and He and metals in atomic form (e.g. C, O, Si). The code propagates ionizing packets with N_γ photons per frequency along rays crossing an arbitrary gas distribution mapped on to a Cartesian grid of N_c^3 cells. At each cell crossing, CRASH evaluates the optical depth τ along the casted path and the number of absorbed photons $N_{\rm abs} = N_\gamma(1 - e^\tau)$. $N_{\rm abs}$ is used to calculate the ionization fractions of the species $x_{\rm gas} = x_{\rm i} \in (x_{\rm H\,II}, x_{\rm He\,II}, x_{\rm He\,III})$ and the gas temperature $T_{\rm gas}$ of the crossed cell.

A CRASH simulation is defined by assigning the initial conditions on a regular 3D Cartesian grid and a physical box linear size of L_b, specifying:

(i) the number density of H ($n_{\rm H}$) and He ($n_{\rm He}$), the gas temperature ($T_{\rm gas}$) and the ionization fractions ($x_{\rm i}$) at the initial time t_0;[1]
(ii) the number of ionizing point sources (N_s), their position in Cartesian coordinates, ionization rate ($\dot{N}_\gamma$ in photons s^{-1}) and spectral energy distribution (S_ν in erg s^{-1} Hz^{-1}) assigned as an array whose elements provide the relative intensity of the radiation as frequency bins;
(iii) the simulation duration (t_f) and a given set of intermediate times ($t_j \in \{t_0, \ldots, t_f\}$) to store the values of the relevant physical quantities;
(iv) the intensity and spectral energy distribution of background radiation, if present.

The interested reader can find more technical information about the latest implementation of CRASH and references about its variants in Graziani et al. (2013).

2.3 Radiation sources

As explained above, CRASH requires the list of all the ionizing sources present in the box grid. This is provided in the GAMESH framework by the GAMETE-to-CRASH module I_0, which is responsible for converting the properties of the SFGs (Pop II/Pop III SFR, Z_*) into CRASH sources with specific spectral properties.

I_0 first maps the centre of mass of each galaxy on to grid coordinates and then converts the SFRs into spectrum-integrated quantities $\dot{N}_\gamma$ depending on the stellar population.

For Pop II stars, we calculate ionization rates and spectral shapes according to Bruzual & Charlot (1993) and we assume an IMF in the mass range [0.1–100] $M_\odot$. A different spectral shape and ionization rate are then associated with each of the Pop II SFGs depending on their population lifetimes t_* and stellar metallicity Z_*. The spectrum and ionization rate are derived from a grid of pre-computed spectra integrated in specific lifetime bins $t_* \in \{0.001, 0.01, 0.1, 0.4, 1.0, 4.0, 13.0\}$ Gyr and stellar metallicity $Z_* \in \{0.005, 0.2, 0.4, 1.0, 2.5\}\,Z_\odot$.

For Pop III stars, we assume an ionization rate per solar mass, $\dot{N}_\gamma = 1.312 \times 10^{48}$ [photons s^{-1} $M_\odot^{-1}$] (Schaerer 2002) corresponding to a stellar mass $M_* \sim 200\,M_\odot$, averaged over a lifetime of about 2.2 Myr. The spectral energy distribution of Pop III stars is simply assumed to be a blackbody spectrum at temperature $T_{\rm BB} = 10^5$ K.

2.4 Radiative feedback

The radiative feedback for SF is implemented by the pipeline module I_1. This module is responsible for setting up the ionization and temperature ($x_{\rm gal}$, $T_{\rm gal}$) of the gas in the galaxies, which are successively processed by GAMETE to establish their SF.

At the first red shift z_0, it is simply assumed that the medium is fully neutral (i.e. $x_{\rm gal} = 0$) and $T_{\rm gal} = T_0(1 + z_0)$, where T_0 is the value of the cosmic microwave background temperature at $z = 0$. During the red-shift iterations, I_1 computes $x_{\rm gal}$ and $T_{\rm gal}$ by first finding the cell containing the galaxy centre of mass in the CRASH grid. In the second step, it evaluates which of the surrounding cells best describe the environment from which the galaxy can get the gas to fuel SF.

The effective environment scale from which cold gas is fuelled into SFGs is crucial for calculating the values of $x_{\rm gal}$ and $T_{\rm gal}$, and for applying the radiative feedback. Since in our pipeline the gas distribution surrounding haloes relies on the spatial resolution of the RT (i.e. the cell size in CRASH: $\Delta L = L_b/N_c$), we compare the virial radius $R_{\rm vir}$ of the galactic halo with $\Delta L/2$. We simply assume that if $2R_{\rm vir}/\Delta L \leq 0.1$, the galactic environment is mainly set up in the cell containing its centre of mass and we assign $x_{\rm gal} = x_{\rm cell}$ and $T_{\rm gal} = T_{\rm cell}$. When, on the other hand, $2R_{\rm vir}/\Delta L > 0.1$ the gas reservoir of the galaxy could extend to the surrounding cells and then $T_{\rm gal}$ is assigned to their volume-averaged value; the value of $x_{\rm gal}$ remains instead that taken from the central cell. It should be noted though, that the threshold 0.1 depends on the resolution of the CRASH grid and must be tuned for grids with increased resolution, when necessary.[2]

Once the temperature and ionization fractions affecting the galactic SF have been assigned, we first use $x_{\rm gal}$ to evaluate the mean molecular weight μ of the gas and then to calculate the virial temperature of the galactic halo $T_{\rm vir}$ (see the formulas in Barkana & Loeb 2001).

SF in the galaxy is finally allowed in GAMETE if $T_{\rm gal} < T_{\rm vir}$, and accretion of cold gas in the galaxy forms stars. In the next version of GAMESH, we will refine the SF prescription to account also for gas cooling, metallicity dependence and dynamical timescales following the approach described in Noh & McQuinn (2014); also see the Introduction for more references and details.

[1] $n_{\rm gas}$ is calculated by projecting the particle distribution of the simulation on a Cartesian grid of N_c^3 cells and by deriving the gas component via the universal baryon fraction.

[2] Improving the accuracy of the galactic environment description would ideally require selectively resolving the halo structures (i.e. a cell size $\Delta L \ll R_{\rm vir}$), as obtained using cell refinements around the galaxies. The spatial resolution adopted in the paper simulation is documented in Section 3.2.

3 MILKY WAY REIONIZATION SIMULATION

Here we describe the set-up of our MW reionization simulation. After a brief description of the *N*-body simulation and its parameters, we detail the RT assumptions and the initial conditions.

Following Scannapieco et al. (2006), we adopt a ΛCDM cosmological model with $h = 0.71$, $\Omega_0 h^2 = 0.135$, $\Omega_\Lambda = 1 - \Omega_0$, $\Omega_b h^2 = 0.0224$, $n = 1$ and $\sigma_8 = 0.9$.

3.1 The *N*-body simulation

To study the MW reionization, we adopt the snapshots and merger tree from a cosmological *N*-body simulation of the MW-sized galaxy halo computed with GCD+ (Kawata & Gibson 2003a), which were used in Scannapieco et al. (2006) and which describes the detail of the simulation; here we briefly summarize the simulation parameters necessary to understand the global GAMESH run.

The mass adopted for the *N*-body particles is $M_\mathrm{p} = 7.8 \times 10^5\,\mathrm{M}_\odot$ and the softening length used is 540 pc. The simulated system consists of about 10^6 particles within the virial radius $R_\mathrm{vir} = 239$ kpc for a total virial mass $M_\mathrm{vir} = 7.7 \times 10^{11}\,\mathrm{M}_\odot$. Note that the virial mass and virial radius estimated by observations for the MW are $M_\mathrm{vir} = 10^{12}\,\mathrm{M}_\odot$ and $R_\mathrm{vir} = 258$ kpc, respectively (Battaglia et al. 2005).

Using a multi-resolution technique (Kawata & Gibson 2003b), the initial conditions at $z = 56$ are set up to resolve the region in a sphere within the radius $R = 4R_\mathrm{vir}$ with the high-resolution *N*-body particles of mass $M_\mathrm{p} = 7.8 \times 10^5\,\mathrm{M}_\odot$ and with the softening length of 540 pc; the other region is resolved instead with lower-resolution particles.

The simulation snapshots are provided at regular intervals every 22 Myr between $z = 8$ and 17 and every 110 Myr for $z < 8$. The virialized DM haloes are then identified with a friend-of-friend group finder by assuming a linking parameter $b = 0.15$ and a threshold number of particles of 50; the resulting minimum mass halo is $M_\mathrm{h} = 3.75 \times 10^7\,\mathrm{M}_\odot$.

A validating *N*-body simulation at lower resolution, also including a SF recipe, has also been performed to confirm that the assumed initial condition led to disc formation (see Brook et al. 2007).

3.2 The RT set-up

The RT simulation is performed at each red shift z_i, on a box size of $2\,h^{-1}$ Mpc comoving, by emitting $N_\mathrm{p} = 10^6$ photon packets from each SFG.[3] The box is mapped on a Cartesian grid of $N_\mathrm{c} = 128$ cells per cube side, providing a cell resolution of $\Delta L \sim 15.6\,h^{-1}$ kpc. The gas in the box is assumed of cosmological composition (92 per cent H and 8 per cent He) and we neglect the metal ions and the effects of the metal cooling around the star-forming haloes. We defer to a future application the extension of GAMESH to the metal ions. For a gas of cosmological composition ($n_{\mathrm{H\,I}} \sim 92$ per cent n_gas), the ionizing spectrum is usually assigned in the energy range 13.6 eV$\leq E_\gamma \leq$ 140 eV. Note that the spectral database could be extended at any time to include harder spectra accounting for sources emitting higher-energy photons. Note also that the CRASH calculation adopts the same cosmological parameters as in the *N*-body simulation to maintain consistency across the pipeline life cycle.

[3] Note that according to the pipeline algorithm each source could have an a priori different spectrum assigned by I_0 as a function of its lifetime and stellar metallicity.

The convergence of the Monte Carlo sampling is guaranteed by an identical run with a factor of 10 larger N_p and providing the same numbers to within the fourth decimal of the volume-averaged ionization and temperature created in the box.

The simulation starts at $z_0 \sim 16$.[4] It has uniform temperature $T_0 \sim 46$ K and we assume that the reionization is completed when the volume-averaged ionization fraction of the hydrogen reaches $x_{\mathrm{H\,II}} \geq 0.995$ against the gas recombination. Due to the large excursion in Hubble time, gas recombination with CASE-B is adopted in the simulation and diffuse re-emission is neglected.

In the absence of a model for the UVB on the scale of the MW formation, we avoid using an external cosmological UVB as done in other works in the literature, and prefer to mimic a flux entering our box by applying periodic boundary conditions to the escaping radiation. While this choice guarantees that the photon mean free path is conserved when the box ionization is advanced and the gas becomes transparent to the hydrogen-ionizing radiation, it should be noted that we do not account for an external ionizing flux likely emitted by the background of Quasi-stellar objects (QSO) sources established below $z \sim 4$.

4 RESULTS

In this section we discuss the results of our simulation, also comparing them with trends obtained adopting the assumption of IReion at $z \sim 6$ as discussed in SF10. Hereafter, for simplicity, we omit the label 'gas' in the variable names referring to ionization fractions and the temperature of the gas and we comment on the single ionized species $x_\mathrm{i} \in (x_{\mathrm{H\,II}}, x_{\mathrm{He\,II}}, x_{\mathrm{He\,III}})$.

4.1 Reionization and temperature histories

Here we investigate the evolution in red shift of the volume-averaged ionization fractions and temperature (in this section $x_i(z)$ and $T(z)$) resulting from the RT simulation.

In Fig. 2 we show the red-shift evolution of $x_{\mathrm{H\,II}}$ (top panel) and $x_{\mathrm{He\,II}}$ and $x_{\mathrm{He\,III}}$ (second and third panels from the top) down to $z = 5$.[5] $x_{\mathrm{H\,II}}$ remains below $x_{\mathrm{H\,II}} \sim 0.1$ when $z > 12$, afterwards it rapidly rises to $x_{\mathrm{H\,II}} \sim 0.5$ at $z \sim 11$ and reaches $x_{\mathrm{H\,II}} \sim 0.9$ when $z \sim 10$. The sudden increase in the hydrogen ionization fraction in the red-shift range $10 < z \leq 12$ can be ascribed both to the rising comoving SFR (Fig. 4) and to the total number of emitting galaxies (Fig. 5) but more likely to an advanced stage of overlapping of ionized regions, which makes the reionization process intrinsically non-linear.

Below $z \sim 10$, the hydrogen reionization continues and $x_{\mathrm{H\,II}}$ increases up to 0.99 by $z \sim 9$ and up to 0.999 by $z \sim 5$. Even if not visible in the figure, below $z \sim 8.5$ the value of the third decimal of $x_{\mathrm{H\,II}}$ continues to oscillate for $0.997 \leq x_{\mathrm{H\,II}} \leq 0.999$ due to the continuous imbalance in gas ionization, created by the ongoing gas collapse, which enhances the recombination rate at the centre, and by the inhomogeneous reionization/recombination in the volume. We consider the hydrogen reionization to be complete at $z \sim 6.4$ when $x_{\mathrm{H\,II}} > 0.995$, neglecting these fluctuations.

[4] This is the first red shift in which the applied Friend-of-Friend (FoF) is able to identify the first haloes. This red shift depends on the mass resolution of the simulation.

[5] Below this red shift, a uniform ionized pattern of hydrogen is created and the values are less indicative. Note that we cannot discuss the helium reionization due to the absence of a harder radiation background.

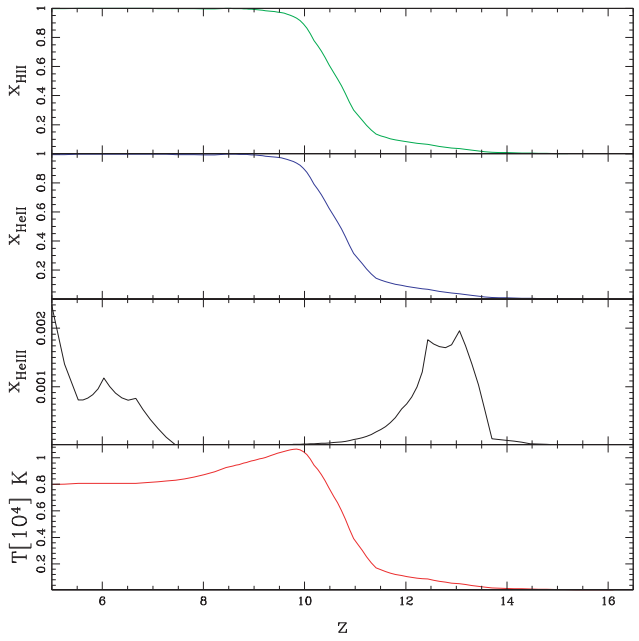

Figure 2. Red-shift evolution of the volume-averaged ionization fractions and temperature of the gas, down to $z \sim 5$. From top to bottom the values of $x_{\rm H\,II}$, $x_{\rm He\,II}$, $x_{\rm He\,III}$, $T[10^4]$ K are shown with solid green, blue, black and red lines, respectively.

The second and third panels from the top of Fig. 2 show the ionization histories of helium. It is immediately evident that He II reionization can be sustained only by the Pop II stars, which dominate below $z \sim 12$, while the reionization of He II never occurs at the considered MW scale (here $2\,h^{-1}$ Mpc comoving) without the contribution of an external background of harder spectra (e.g. QSO). In fact, while the red-shift trend for $x_{\rm He\,II}$ follows that of the hydrogen, $x_{\rm He\,III}$ never reaches higher than $x_{\rm He\,III} = 0.002$ along the entire red-shift range. As also pointed out for $x_{\rm H\,II}$, the volume-averaged ionization fraction of He II continues to oscillate in $0.97 < x_{\rm He\,II} < 0.99$ below $z \sim 8.5$, confirming that a harder spectral component is required to sustain full helium ionization against gas recombination. Note that a bump in the value of $x_{\rm He\,III}$ (third panel from the top) occurs in the red-shift range $12 < z < 15$, tracing the presence of Pop III stars (see also Fig. 4) with their harder spectral shapes. Note also that the volume-averaged value of $x_{\rm He\,III}$ is always negligible over the entire simulation: after the transition from Pop III to Pop II stars the presence of fully ionized helium is so closely confined to the sources that it is not visible in the panel, except at $z < 7$, when hydrogen ionization is complete and harder photons ($E_\gamma > 54.4$ eV) are free to cross the box many times and to create a very small ionization fraction of fully ionized helium.

The red-shift evolution of the volume-averaged temperature is shown in the bottom panel of Fig. 2 to a [10^4 K] scale. Before $z \sim 10$, the temperature rises from the initial value $T \sim 50$ K up to $T \sim 10^4$ K; note that the rapid evolution of Pop III stars in this red-shift range is so small (not visible in the plot) that it cannot change the global trend of the average temperature. In the red-shift interval $9 < z < 10$, the gas stabilizes at an average photo-ionization equilibrium temperature of $T \sim 10^4$ K, before its average value starts decreasing by some 10^3 K during the successive evolution. Oscillations of the order of 10^3 K are present below $z \sim 5$ (not shown in the plot), due to the competitive effects of gas clumping towards the centre, adiabatic cooling due to the cosmological expansion, and finally inhomogeneous distribution and the properties of the ionizing galaxies. Even if not visible in this plot we report a final average temperature of $T = 7.9 \times 10^3$ K at $z = 0$, but recall that this value is certainly underestimated in our simulation due to the absence of high-energy photons from the QSO background established at a large-scale below $z \sim 4$.

To illustrate visually how the reionization process evolves in space and red shift, we show in Fig. 3 three slice cuts of our volume (of $2\,h^{-1}$ Mpc comoving side length) taken at red shifts $z \sim 12$, 11 and 6 (see panels from top to bottom). Panels in the first column show $\log(n_{\rm gas}(z))$ as a grey gradient from black ($n_{\rm gas} \sim 2 \times 10^{-5}$ cm^{-3}) to white ($n_{\rm gas} \sim 0.4$ cm^{-3}); in the second column $x_{\rm H\,II}(z)$ is shown by a colour palette from white ($x_{\rm H\,II} < 10^{-5}$) to dark blue ($x_{\rm H\,II} = 1.0$), and finally the pattern for $T(z)$ is drawn in the third column with a different colour palette from light red ($T \sim 50$ K) to dark red ($T \sim 1.9 \times 10^4$ K). In all the panels, the distances are shown in cell units ($\sim 15.6\,h^{-1}$ kpc per cell) along the x and y directions.

Superimposed on the number density maps, we also show the SFGs present in the surface of choice: galaxies forming Pop III stars are symbolised as blue crosses (top panel), while gold-yellow asterisks are for Pop II stars. Also note that the size of each symbol is scaled with $\dot{N}_\gamma$ and the position of SFGs correlates perfectly with the gas filaments falling towards the centre where the central galaxy is progressively forming along the red-shift evolution.

As a consequence of the central position of the ionizing sources, the reionization proceeds inside out. At high red shift (top panels), the low-density regions surrounding the centre of the box (black regions, first column) are easily ionized by the sources (blue pattern, second column). At the centre of the image note that high-density clumps (white regions) are able to suppress photo-ionization with a high gas recombination rate (light blue patterns). The average gas temperature (third column) tends to stabilize around $T \sim 1.4 \times 10^4$ K in the regions involved in the overlap of ionized bubbles (light and dark red), mainly driven by the contribution of Pop III stars. T rapidly decreases down to $T \sim 10^2$ K at the border of the ionized region (light red patterns) not reached by stellar radiation. Consistent with the ionized pattern, few high-density structures remain self-shielded and settle at very low temperature in the centre image. Note that the presence of helium in our simulation significantly changes the gas photo-heating by enhancing the contrast between over-dense regions and voids. At $z \sim 11$ (middle row) the reionization is already quite advanced and the ionizing radiation involves a large fraction of the box, including the under-dense regions far away from the centre (light blue patterns). Voids are rapidly ionized and their temperature stabilizes around $T \sim 6 \times 10^3$ K, well below the central value $T \sim 10^4$ K. Finally, at $z \sim 6$ the entire volume reaches photo-ionization equilibrium and its average temperature stabilizes around $T \sim 8.0 \times 10^3$ K but the spatial pattern continues to show large variations from the gas filaments (branching off the central MW-type galaxy) and from the under-dense regions.

Note that at the final red shift ($z \sim 6.1$), the central galaxy is a single source with the highest ionization rate about $\dot{N}_\gamma = 2 \times 10^{54}$ photons s^{-1} and SFR $\sim 13\,{\rm M}_\odot$ yr^{-1} (the total SFR of the emitting objects is $\sim 20\,{\rm M}_\odot$ yr^{-1}). In the other galaxies lying on the plane, SF is suppressed by radiative feedback (see Section 4.2.1 for more details).

As a final comment, we point out that our simulation lacks the ionizing contribution of an external UVB, especially at the helium-ionizing frequencies. While periodic boundary conditions are adopted to preserve the photon mean free path at all frequencies, the external UVB may play a relevant role because of the small

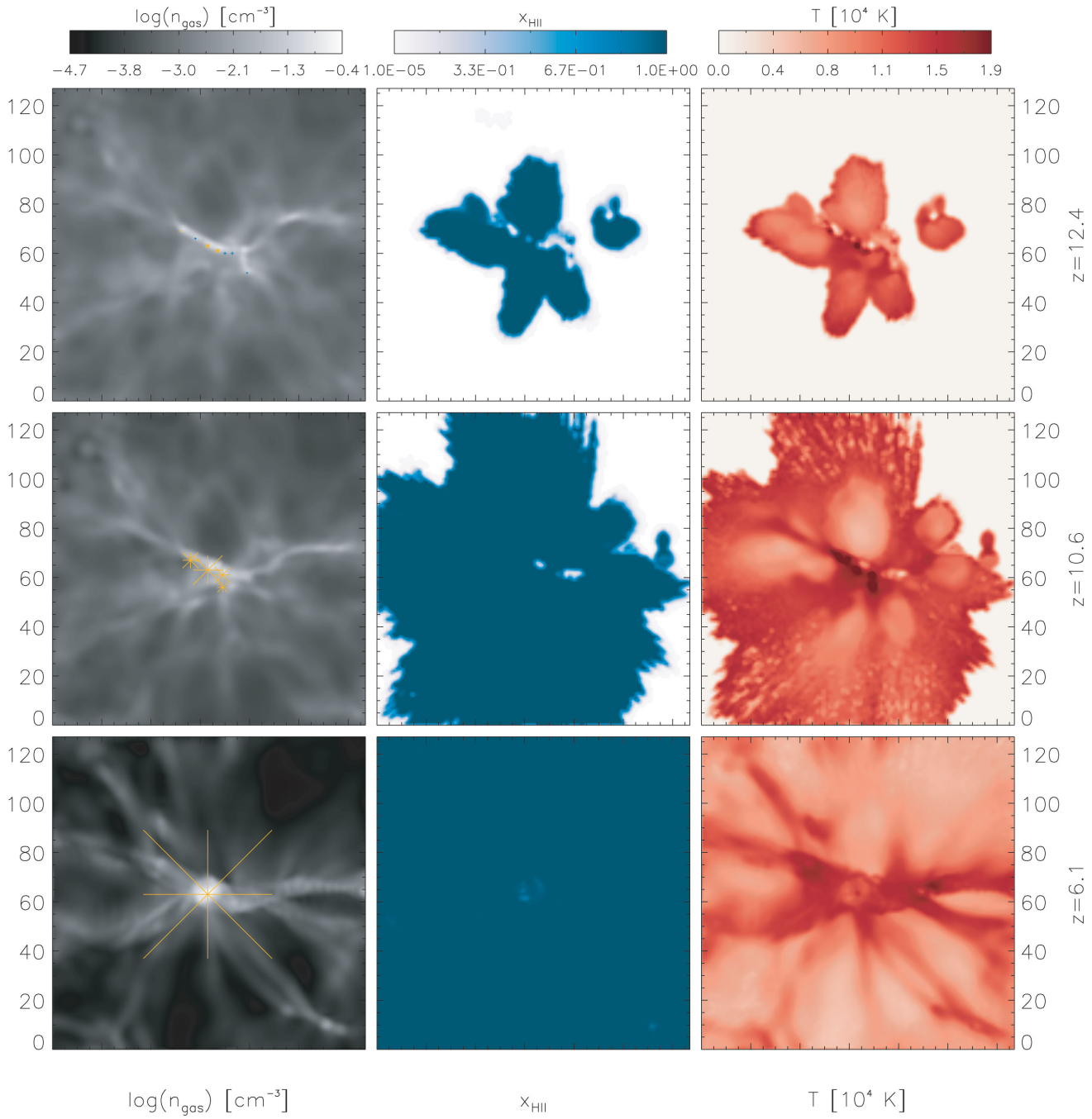

Figure 3. Slice cuts of $n_{\rm gas}$ (first column), $x_{\rm H\,II}$ (second column) and T (third column) at three different red shifts: $z \sim 12$ (top panels), $z \sim 11$ (middle panels) and $z \sim 6$ (bottom panels). The values of the fields in the planes are represented as colour palettes and the distance units are represented by the marks along the x- and y-axes ($\sim 15.6\,h^{-1}$ kpc per cell). In the first-column panels, SFGs are symbolised as blue crosses when forming Pop III stars and gold-yellow asterisks for Pop II stars; the sizes of the symbols are scaled with the galaxy ionization rate $\dot{N}_\gamma$

size of the simulation box and its coarse mass resolution. On the other hand, the inclusion of a UVB is neither trivial nor straightforward. First, the available UVB models (see for example Haardt & Madau 2012 and references therein) are computed and calibrated on the large-scale structure. Therefore, on the scales of MW formation, both the intensity and the spectral shape of the UVB may be modified by RT effects. Using the radiation tracking features of CRASH3, we will investigate these effects in a future study. Here we only point out that an external UVB could only impact hydrogen ionization above $z \sim 11$. In fact, Fig. 2 shows that below this red shift the internal flux is sufficient to sustain hydrogen ionization.

4.2 Feedback on star formation

The red-shift evolution of the comoving SFR is shown in Fig. 4, where the red lines refer to the contribution from Pop II stars (highest curve) and the blue lines to Pop III. Dotted lines, with the same colours, show the values obtained by adopting the instantaneous

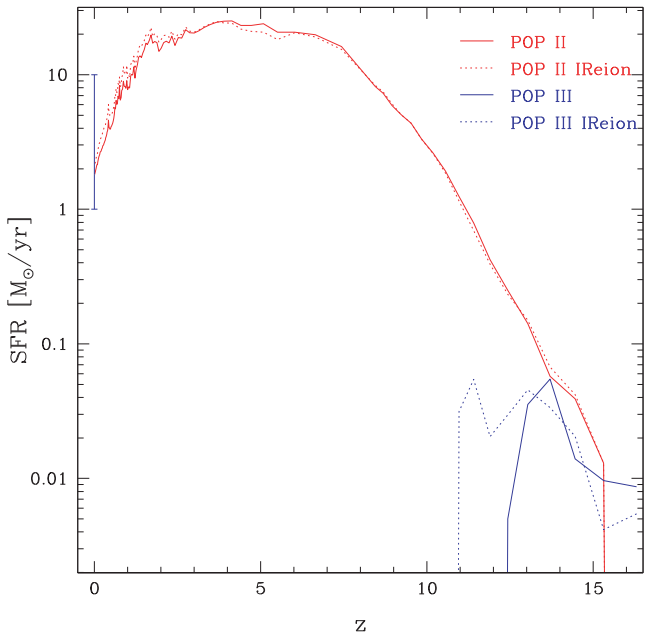

Figure 4. Star-formation rate for Pop II (solid red lines) and Pop III (solid blue) as a function of z. As a reference, the values obtained with the IReion approximation are shown as dotted lines in the same colours for the two populations. The value of the SFR estimated by observation at $z = 0$ is reported as an error bar. See text for more details.

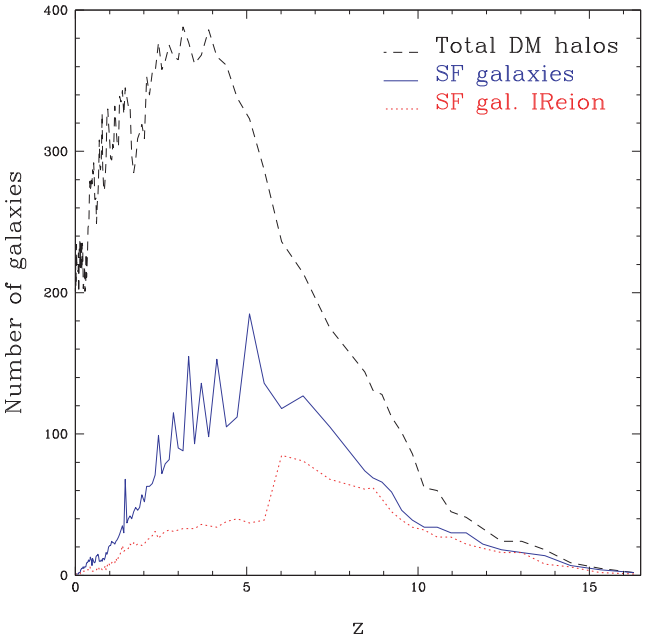

Figure 5. Number of SFGs as a function of z from the simulation (solid blue line). The dotted red line refers to the IReion case, while the dashed black line shows, as a reference, the total number of DM haloes found in the N-body simulation.

reionization prescription (See Section 2.1). In the red-shift interval $12.4 < z \lesssim 16$, the total SFR of our simulation (solid lines) increases up to $1.7\,\mathrm{M}_\odot\ \mathrm{yr}^{-1}$ thanks to both Pop III and Pop II stars, but note that at the highest red shift $z \sim 16.5$ (when the gas is mostly primordial) only Pop III objects contribute to the total SFR. Feedback from Pop III forming galaxies, both radiative and chemical, acts efficiently on the surrounding medium: their hard spectra locally increase the MWenv temperature inhibiting SF in unpolluted clouds, while mechanical feedback rapidly pollutes the MWenv up to the critical metallicity $Z_{\rm cr} = 10^{-4}\,\mathrm{Z}_\odot$. Both effects contribute to their sudden disappearance, triggering the formation of Pop II stars below $z \sim 12.4$. At lower red shift, Pop II stars cause an increase of the total SFR up to a value of SFR $\sim 25\,\mathrm{M}_\odot\ \mathrm{yr}^{-1}$ at the peak red shift $z \sim 4$. The successive evolution proceeds with an irregular but progressive decrease down to a value of SFR $\sim 1.8\,\mathrm{M}_\odot\ \mathrm{yr}^{-1}$ at $z = 0$, in good agreement with the observed data (Chomiuk & Povich 2011).

It is interesting to compare these results with those obtained with the IReion approximation for both populations. Recall that in the IReion approximation, GAMETE accounts for feedback by assuming that only Lyman-α haloes having $M_h > M_4$ can form stars at $z > 6$, while at $z \sim 6$ the volume is suddenly ionized and a different threshold applies. For $z < 6$, only haloes with circular velocity greater than $30\,\mathrm{km\,s}^{-1}$ (i.e. $M_h > M_{30}$) can trigger SF (see SF10).

By comparing the solid and dotted lines in Fig. 4, we immediately conclude that the suppression of SF by IReion is quite appropriate for reproducing the SFR of Pop II stars in a wide red-shift range but it overestimates the SFR at $z = 0$ by 15 per cent. Note also that the stronger radiative feedback effects at high red shift with IReion lower the SFR of Pop III stars and delay the transition between the two stellar populations.

4.2.1 *Feedback statistics*

The effects of the radiative feedback on the statistics of SFGs are shown in Fig. 5 as a function of red shift z. The solid blue line indicates the number of SFGs computed in our simulation, while the dotted red line refers to the IReion case. The total number of DM haloes found in the N-body simulation in use is shown as a dashed black line.

By comparing the solid and dotted lines, we first note that at the current resolution of the simulation, which does not resolve the full range of masses that sample the mini-halo regime, the condition $M_h > M_4$ could appear quite appropriate to reproduce the statistics of the galaxies with suppressed SF at very high red shifts ($z > 10$). On the other hand, a careful comparison with Fig. 4 immediately shows the different SFRs of Pop III galaxies (compare the blue lines in Fig. 4).

This discrepancy can be ascribed to a combination of reasons that involve radiative, mechanical, and chemical feedback. Also note that the IReion model cannot account for inhomogeneous feedback on high-red-shift low-mass objects (which are likely to host Pop III stars) but indiscriminately applies to *all* the galaxies with $M_h > M_4$ present in the volume. At high red shift, this assumption is particularly incorrect because the SFGs are still quite separated in space and then their radiative feedback acts very selectively, only affecting their surrounding neighbourhoods. See for example how dishomogeneous is the bubble overlap in the third column of Fig. 3 and how many regions of the simulated volume remain unaffected by photo-heating.

Note that the current mass resolution of the N-body simulation does not allow us to draw robust conclusions about the radiative feedback effects at high-red shift. This will be the subject of a future dedicated study (de Bennassuti et al., in preparation).

At lower red shifts, the efficiency of the radiative feedback increases with the progress of reionization in both models. In the red-shift interval $6 < z \lesssim 9$, the GAMESH run predicts that around

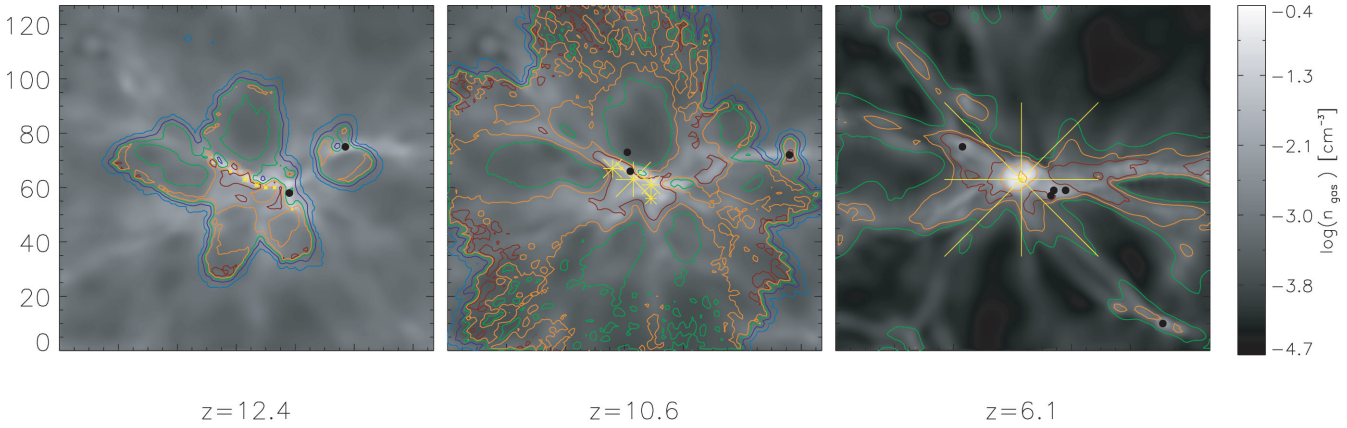

Figure 6. Slice cuts of the gas number density $n_{\rm gas}$ with superimposed temperature contour plots: $T \sim 100$ K (cyan), $T \sim 4 \times 10^3$ K (blue), $T \sim 10^4$ K (green), $T \sim 1.3 \times 10^4$ K (orange) and $T \sim 1.5 \times 10^4$ K (dark red). All the star-forming haloes in the plane are represented by yellow asterisks, while black dots indicate haloes in the plane in which SF is suppressed by radiative feedback.

50 per cent of the galaxies have been affected by radiative feedback and this value increases up to 65 per cent by $z \sim 4$, with a jagged trend due to both oscillations in the number of potential galaxies (dashed black line in Fig. 5) and the inhomogeneous heating in space induced by the RT.[6] Below $z = 4$, the suppression of SF in small galaxies progresses rapidly, allowing few remaining objects in the box to form stars, as observed in the MW environment.

Note the difference in the statistics for SFGs below $z \sim 6$ obtained with the IReion approximation. In fact a realistic radiative feedback operates with a more gradual suppression in time, due to the inhomogeneous nature of the bubble overlap in space. For $3 < z < 6$, this difference induces an error in the number of SFGs as high as 40 per cent between the two cases (compare the solid blue line to the dotted red line in Fig. 5). On the other hand, this statistical discrepancy between models is not reflected in both the total SFR (Fig. 4) and the MWenv enrichment (see Fig. 8), which are very similar in this red-shift range, also indicating that the high-mass galaxies surviving the IReion prescription provide a dominant contribution to these quantities.

Fig. 6 visually shows how the inhomogeneous radiative feedback operates in space, in comparison with the same slice cuts and red-shift sequence of Fig. 3. Here, on top of the gas number density field we have traced a few solid line iso-contours of the gas temperature: $T \sim 100$ K in cyan, $T \sim 4 \times 10^3$ K in blue, $T \sim 10^4$ K in green, $T \sim 1.3 \times 10^4$ K in orange and finally $T \sim 1.5 \times 10^4$ K in dark red. All the SFGs are symbolised by yellow asterisks, while the galaxies in which SF has been suppressed by radiative feedback are shown as black filled circles.

By comparing the three panels, it is immediately evident how the inhomogeneities in the reionization induce large differences in randomly suppressing SF (left and middle panels) before UVB is fully established (right panel). At high red shifts, a few suppressed SFGs (black circles) are trapped in regions with $T \sim 10^4$ K, not necessarily connected with the emitting galaxies. Note for example the galaxy on the right side of the middle panel: even far from the centre it is surrounded by gas at a high temperature, which likely originates from complicated 3D effects created by the RT. On the other hand, at $z \approx 6$ (right panel) the medium is already pervaded by a quasi-homogeneous UVB and then all the galaxies below a critical mass are easily suppressed in the entire domain. To study if a critical mass for the suppression of SFGs is statistically restored against the non-linearity induced by the RT, we should rely on a higher resolution simulation providing better statistics for both Lyman-α and H_2-cooling haloes, as well as better spatial resolution. With this study we will able to provide a numerically motivated recipe for semi-analytic models. We then defer this point to the next work (de Bennassuti et al., in preparation) and limit the discussion to this figure, as an illustrative example of how radiative feedback implemented in GAMESH works.

4.2.2 *Local versus environmental feedback*

As introduced in Section 2.4, the radiative feedback defined in GAMESH depends on the spatial extension of the galactic environment feeding cold gas for SF. Depending on the virial radius of the DM halo hosting each galaxy and the spatial resolution of the RT grid, the feedback could act *locally* to the sources (i.e. accounting just for the temperature in the galaxy cell ($2R_{\rm vir} \leq 0.1\Delta L$)) or it could act *globally* involving larger scales (i.e. cells surrounding the one containing the galaxy) when $2R_{\rm vir} > 0.1\Delta L$.

The statistics of these two mechanisms can help us to understand the importance of local versus global feedback during reionization in establishing a H-ionizing uniform UVB. In Fig. 7 we show the percentage of SFGs (solid black line) together with the percentage of galaxies that are influenced by local feedback (dashed red line).[7] To understand which stellar population is affected by local or environmental effects, we also show as a blue dotted line the percentage of galaxies forming Pop II stars.

As already noted for Fig. 7, the percentage of SFGs (solid black line) rapidly decreases from high to low red shifts during reionization with a spiky and irregular trend down to $z \sim 4$. The presence of a plateau in the red-shift interval $6 < z < 9$ could mark the existence of an extended reionization epoch in which the gas is kept in photo-ionization equilibrium in the entire box at $T \sim 10^4$ K and the hydrogen ionization fraction increases from 0.99 up to 0.999. The dashed line indicates that isolated high red-shift galaxies ($z > 12.4$)

[6] As noted in the previous paragraph, only with a higher mass and spatial resolution simulation can we fully understand the impact of an inhomogeneous reionization process on the statistics of SF galaxies.

[7] These numbers are calculated with respect to the total number of haloes found in the simulation.

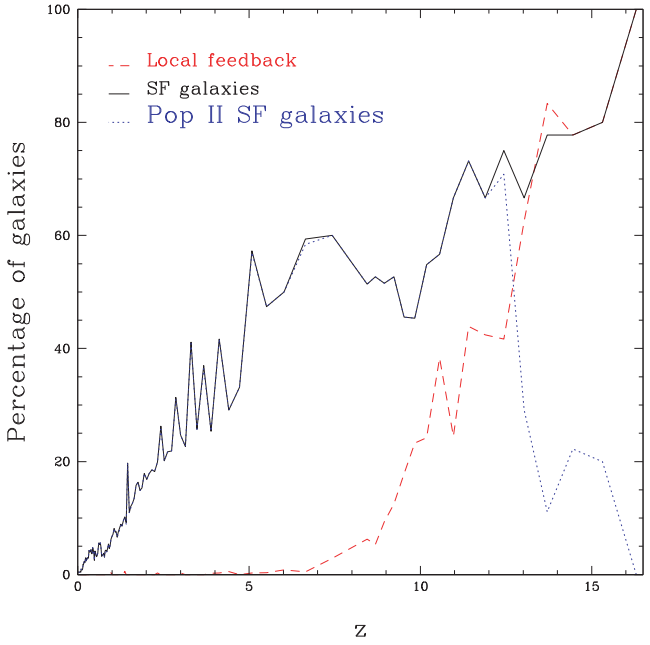

Figure 7. Percentage of SFGs as a function of z (solid black line) and percentage of galaxies affected by radiative feedback in their own cell (dashed red line). The blue dotted line shows the percentage of galaxies forming mainly Pop II stars.

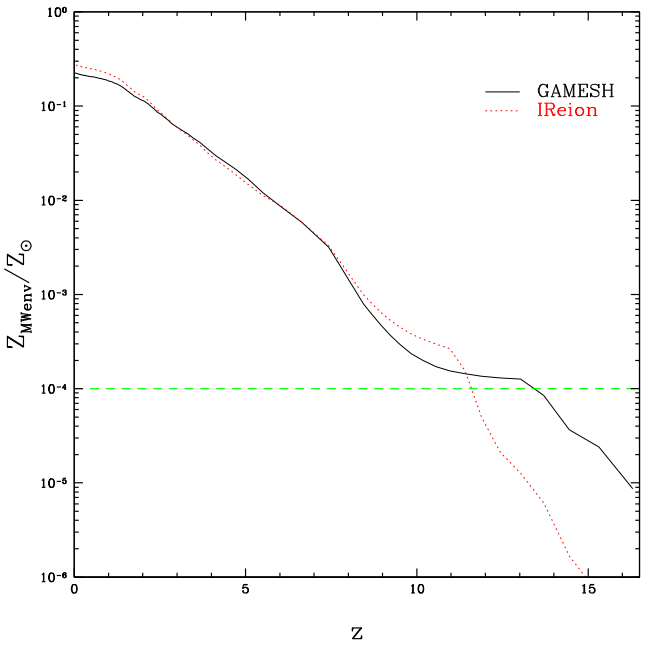

Figure 8. Evolution in red shift of the MW environment metallicity Z_{MWenv} (solid black line) in solar metallicity units. The values obtained by assuming IReion are shown with the dotted red line. The green dashed line shows, as a reference, the value adopted for the critical metallicity to form Pop II stars.

are quite insensitive to their environment and that radiative feedback plays only a local role. A quick comparison with the blue dotted line clearly shows that these galaxies mainly form Pop III stars. After the population transition, Pop II forming galaxies are instead progressively affected by their environment: below $z \sim 8$, both the increase of the virial radii of the sources and a more uniform ionizing background make the environment progressively more important and the feedback acts globally. At these red shifts the gas temperature is sustained by: (i) the few satellite galaxies surviving radiative feedback, (ii) the global UVB entering the box, and (iii) the predominant emission from the central MW-type galaxy. It is in fact clear from Fig. 7 that less than 40 per cent of galaxies are capable of accreting gas from the surrounding reservoir to fuel the SF process below $z \sim 4$.

4.3 Interplay with chemical feedback

In this section we briefly investigate how the reionization can leave specific signatures in the chemical evolution of the MW environment and in the final properties of the MW at $z = 0$ and, in particular, of the most metal-poor stars observed in the Galactic halo.

In Fig. 8 we show the red-shift evolution of the MWenv metallicity Z_{MWenv}[8] predicted by GAMESH (solid black line) and the corresponding values obtained by assuming IReion (dotted red line). As already noted for Figs 4 and 5, the SF history of Pop III stars is remarkably different when an accurate model for the radiative feedback is used and their rapid burst, predicted by our simulation, is clearly imprinted in the metallicity of the diffuse, external medium. In fact, Z_{MWenv} experiences a rapid increase at high red shift, reaching the critical value $Z_{cr} = 10^{-4}\,Z_\odot$ by $z \sim 14$.

[8] This value is defined as the metallicity of the medium surrounding the collapsed haloes and it is calculated as the ratio of the mass of metals over the total mass of the gas.

After a flat evolution corresponding to the Pop III to Pop II transition, the increasing trend is restored by the increase in SFR of Pop II stars. As for the SFR (see Fig. 4), Z_{MWenv} becomes consistent with the value predicted by the IReion case in the red-shift interval $3 < z \leq 8$ after which it flattens. Note that a 15 per cent difference in the SFR at $z = 0$ due to extended reionization is reflected in a 25 per cent decrease of the final metallicity Z_{MWenv}.

It should be noted that the trend at high red shift is certainly unphysical because the metallicity of the medium surrounding the galaxies on our box scale is expected to increase more progressively in red shift from very low Z_{MWenv} as correctly predicted by the IReion model. We thoroughly investigated what causes this trend, finding a concurrence of reasons. First, our N-body simulation does not provide a sufficient mass resolution for accurately predicting the distribution of low-mass mini-haloes, which are expected to have played a relevant role in the early metal enrichment of the MW and its dwarf satellites (see for example Salvadori & Ferrara 2009; Sales et al. 2014; Salvadori et al. 2014). As a consequence GAMESH tends to overestimate the production and dispersion of metals in the first star-forming objects. Second, as indicated by pure semi-analytic calculations that simultaneously reproduce different data sets at $z = 0$ (see Salvadori & Ferrara 2012; Salvadori et al. 2014), a better description of both the stellar lifetimes and the inhomogeneous dispersion of metals into the MWenv is required when the effect of inhomogeneous reionization is considered. Finally, for the radiative feedback, the extension of the frequency range to a Lyman–Werner frequency band is necessary to reproduce the SF correctly in H_2-cooling haloes.

The MDF of ancient stars in the final MW-like galaxy clearly reflects the different evolutions of both the total SFR and Z_{MWenv} at $z > 8$–10, where the majority of [Fe/H] < -3 stars are formed (de Bennassuti et al. 2014). In Fig. 9, we compare the MDFs of $z = 0$ stars in the radial range $7 < r < 20$ kpc for the IReion and GAMESH runs. Black points with error bars show the available data

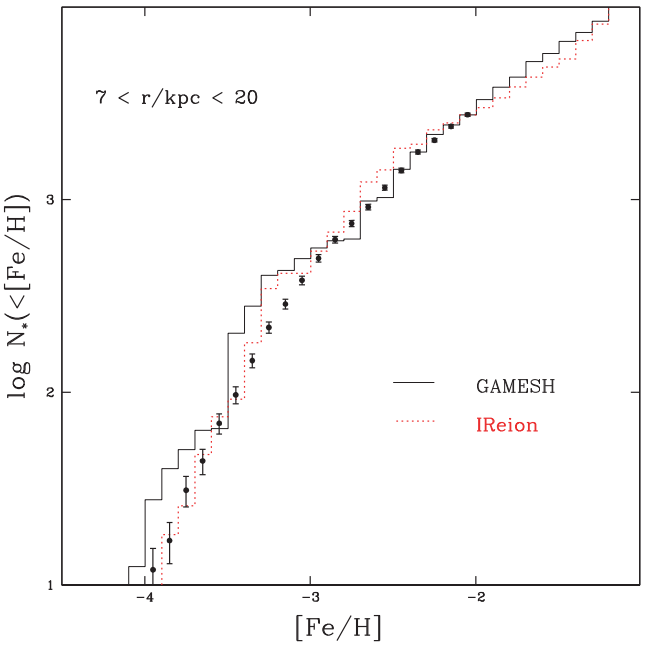

Figure 9. MDF of the central galaxy calculated by GAMESH (solid black line) and in the IReion case (dotted red line) in the radial range $7 < r < 20$ kpc. Black points indicate observed data taken from Beers & Christlieb 2005.

for Galactic halo stars in the same galactocentric ranges (see also SF10).

Both curves show a satisfactory agreement in the overall trend of the observed data, and the differences between the two runs are much smaller than the errors induced when considering different MW merger histories (Salvadori et al. 2007; de Bennassuti et al. 2014). While the GAMESH run fits the data for [Fe/H] > -3 (see Beers & Christlieb 2005), it clearly over-produces the number of low-metallicity stars, [Fe/H] < -3. This is due to the slower progress of metal enrichment, as reflected by the shallow increase of $Z_{\rm MWenv}$ in the red-shift range $8 < z < 13$ (see the plateau in Fig. 8). We interpret this issue as a clear indication that the current resolution of the simulation does not allow us to trace SF and radiative feedback accurately at the highest red shifts.

5 CONCLUSIONS

In this work we investigated the early formation of a MW-like galaxy using GAMESH, a novel tool combining for the first time in the literature an *N*-body simulation with detailed chemical and radiative feedback in a self-consistent framework. Many aspects of the formation have been discussed along the cosmic time, such as the evolution of the SFR, the Pop III to Pop II transition, the statistics of progenitor haloes in which SF is suppressed, and finally the interplay between chemical and radiative feedback in setting up the chemical properties of the Local Group and the final MDF of the Galactic halo.

Even with a low-resolution *N*-body simulation, which lacks statistics and does not allow us to draw definite conclusions for many aspects of the problem, GAMESH has been proven to be an ideal tool for providing both a comprehensive vision of the early formation of the Galaxy and its reionization, and for including an accurate self-consistent treatment of chemical, mechanical and radiative feedback in numerical simulations.

The capability of GAMESH to switch between a pure semi-analytic treatment and inclusion of accurate RT enabled us carefully to compare and contrast all the results obtained by both models and to compare with the observed properties of the Galaxy and the surrounding environment at $z = 0$. In addition, the GAMESH algorithm is very general and its applicability is not limited to MW formation; it can be extended and adapted to a wide range of galaxy- and SF-related topics.

A future work, based on high mass and spatial resolution simulation, is certainly needed to establish accurately the epoch and extension of reionization and its interplay with chemical feedback, the role of mini-haloes and finally the signatures of global feedback processes on the stellar halo MDF and luminosity function of MW satellites.

ACKNOWLEDGEMENTS

The authors would like to thank the anonymous referee for their very constructive comments. LG thanks R. Valiante for the invaluable support during the GAMETE refactoring and re-engineering. SS acknowledges support from the Netherlands Organization for Scientific Research (NWO), VENI grant 639.041.233. RS, AM and SS wish to thank the Osservatorio Astrofisico di Arcetri where the project was originally conceived and developed in successive meetings.

The authors acknowledge Andrea Ferrara and Benedetta Ciardi for their very constructive comments. We also thank the 4C Institute at the Scuola Normale Superiore of Pisa for the computational resources necessary to develop and test GAMESH. We also acknowledge PRACE[9] for awarding us access to the CEA HPC facility CURIE@GENCI[10] under the Type B project: High Performance Release of the GAMESH Pipeline.

The research leading to these results has received funding from the European Research Council under the European Union's Seventh Framework Programme (FP/2007-2013)/ERC Grant Agreement no. 306476.

REFERENCES

Alvarez M. A., Busha M., Abel T., Wechsler R. H., 2009, ApJ, 703, L167
Barkana R., Loeb A., 2001, Phys. Rep., 349, 125
Battaglia G. et al., 2005, MNRAS, 364, 433
Beers T. C., Christlieb N., 2005, ARA&A, 43, 531
Belokurov V. et al., 2006, ApJ, 647, L111
Benson A. J., Frenk C. S., Lacey C. G., Baugh C. M., Cole S., 2002a, MNRAS, 333, 177
Benson A. J., Lacey C. G., Baugh C. M., Cole S., Frenk C. S., 2002b, MNRAS, 333, 156
Bovill M. S., Ricotti M., 2009, ApJ, 693, 1859
Bovill M. S., Ricotti M., 2011a, ApJ, 741, 17
Bovill M. S., Ricotti M., 2011b, ApJ, 741, 18
Boylan-Kolchin M., Bullock J. S., Kaplinghat M., 2012, MNRAS, 422, 1203
Brook C. B., Kawata D., Scannapieco E., Martel H., Gibson B. K., 2007, ApJ, 661, 10
Brown T. M. et al., 2012, ApJ, 753, L21
Bruzual A. G., Charlot S., 1993, ApJ, 405, 538
Busha M. T., Alvarez M. A., Wechsler R. H., Abel T., Strigari L. E., 2010, ApJ, 710, 408
Chomiuk L., Povich M. S., 2011, AJ, 142, 197
Ciardi B., Ferrara A., Marri S., Raimondo G., 2001, MNRAS, 324, 381

[9] http://www.prace-ri.eu/
[10] http://www-hpc.cea.fr/en/complexe/tgcc-curie.htm

Couchman H. M. P., Rees M. J., 1986, MNRAS, 221, 53
D'Onghia E., Besla G., Cox T. J., Hernquist L., 2009, Nature, 460, 605
D'Onghia E., Springel V., Hernquist L., Keres D., 2010, ApJ, 709, 1138
de Bennassuti M., Schneider R., Valiante R., Salvadori S., 2014, MNRAS, 445, 3039
Dijkstra M., Haiman Z., Rees M. J., Weinberg D. H., 2004, ApJ, 601, 666
Efstathiou G., 1992, MNRAS, 256, 43
Gnedin N. Y., 2000, ApJ, 542, 535
Graziani L., Maselli A., Ciardi B., 2013, MNRAS, 431, 722
Haardt F., Madau P., 2012, ApJ, 746, 125
Hoeft M., Yepes G., Gottlöber S., Springel V., 2006, MNRAS, 371, 401
Kawata D., Gibson B. K., 2003a, MNRAS, 340, 908
Kawata D., Gibson B. K., 2003b, MNRAS, 346, 135
Kitayama T., Tajiri Y., Umemura M., Susa H., Ikeuchi S., 2000, MNRAS, 315, L1
Klypin A., Kravtsov A. V., Valenzuela O., Prada F., 1999, ApJ, 522, 82
Koposov S. E., Yoo J., Rix H.-W., Weinberg D. H., Macciò A. V., Escudé J. M., 2009, ApJ, 696, 2179
Kravtsov A. V., Gnedin O. Y., Klypin A. A., 2004, ApJ, 609, 482
Li Y.-S., De Lucia G., Helmi A., 2010, MNRAS, 401, 2036
Li T. Y., Alvarez M. A., Wechsler R. H., Abel T., 2014, ApJ, 785, 134
Lunnan R., Vogelsberger M., Frebel A., Hernquist L., Lidz A., Boylan-Kolchin M., 2012, ApJ, 746, 109
Macciò A. V., Kang X., Fontanot F., Somerville R. S., Koposov S., Monaco P., 2010, MNRAS, 402, 1995
Madau P., Kuhlen M., Diemand J., Moore B., Zemp M., Potter D., Stadel J., 2008, ApJ, 689, L41
Maselli A., Ferrara A., 2005, MNRAS, 364, 1429
Maselli A., Ferrara A., Ciardi B., 2003, MNRAS, 345, 379
Maselli A., Ciardi B., Kanekar A., 2009, MNRAS, 393, 171
Milosavljević M., Bromm V., 2014, MNRAS, 440, 50
Moore B., Ghigna S., Governato F., Lake G., Quinn T., Stadel J., Tozzi P., 1999, ApJ, 524, L19
Muñoz J. A., Madau P., Loeb A., Diemand J., 2009, MNRAS, 400, 1593
Noh Y., McQuinn M., 2014, MNRAS, 444, 503
Ocvirk P. et al., 2014, ApJ, 794, 20
Okamoto T., Gao L., Theuns T., 2008, MNRAS, 390, 920
Sales L. V., Marinacci F., Springel V., Petkova M., 2014, MNRAS, 439, 2990
Salvadori S., Ferrara A., 2009, MNRAS, 395, L6
Salvadori S., Ferrara A., 2012, MNRAS, 421, L29
Salvadori S., Schneider R., Ferrara A., 2007, MNRAS, 381, 647
Salvadori S., Ferrara A., Schneider R., 2008, MNRAS, 386, 348
Salvadori S., Ferrara A., Schneider R., Scannapieco E., Kawata D., 2010, MNRAS, 401, L5 (SF10)
Salvadori S., Tolstoy E., Ferrara A., Zaroubi S., 2014, MNRAS, 437, L26
Sawala T. et al., 2014, preprint (arxiv:1406.6362)
Scannapieco E., Kawata D., Brook C. B., Schneider R., Ferrara A., Gibson B. K., 2006, ApJ, 653, 285
Schaerer D., 2002, A&A, 382, 28
Schneider R., Ferrara A., Natarajan P., Omukai K., 2002, ApJ, 571, 30
Schneider R., Omukai K., Inoue A. K., Ferrara A., 2006, MNRAS, 369, 1437
Schneider R., Salvaterra R., Choudhury T. R., Ferrara A., Burigana C., Popa L. A., 2008, MNRAS, 384, 1525
Sobacchi E., Mesinger A., 2013, MNRAS, 432, L51
Somerville R. S., 2002, ApJ, 572, L23
Springel V. et al., 2008, MNRAS, 391, 1685
Thoul A. A., Weinberg D. H., 1996, ApJ, 465, 608
Tinsley B. M., 1980, Fundamentals Cosmic Phys., 5, 287
Willman B. et al., 2005, AJ, 129, 2692
Zahn O., Mesinger A., McQuinn M., Trac H., Cen R., Hernquist L. E., 2011, MNRAS, 414, 727
Zucker D. B. et al., 2006a, ApJ, 650, L41
Zucker D. B. et al., 2006b, ApJ, 643, L103

This paper has been typeset from a TEX/LATEX file prepared by the author.